

Reliable, high-frequency miniature valves for smart material electrohydraulic actuators

John P Larson and Marcelo J Dapino

Journal of Intelligent Material Systems and Structures
23(7) 805–813
© The Author(s) 2012
Reprints and permissions:
sagepub.co.uk/journalsPermissions.nav
DOI: 10.1177/1045389X12438628
jim.sagepub.com


Abstract

A key element in developing high-performance smart material electrohydraulic actuators is the design of improved check valves for high-frequency fluid rectification. One method to create valves with fast frequency response is to replace the single-reed valves typically used in these systems with an array of miniature-reed valves. A robust miniature-reed design is presented to overcome the fatigue and fabrication limitations observed in previous approaches. The fluid–structure interaction between an individual valve and hydraulic fluid is modeled using the multiphysics software COMSOL; the results are validated with experimental testing on an array of miniature reeds. The performance of this array in a smart material actuator is compared with a larger, single-reed valve design. The miniature-reed array is shown to reliably rectify flow in the high-pressure and high-frequency environment of a smart material pump.

Keywords

Terfenol-D, magnetostrictive pump, reed valves, hydraulic rectification, electrohydraulic actuator

Introduction

Smart material electrohydraulic actuators use hydraulic rectification to take advantage of the high-force and fast-frequency response of smart materials such as piezoelectrics and magnetostrictives; the small, high-frequency pulses of fluid produced by a pump piston are collected with one-way valves. A hydraulic cylinder is integrated with the pump to form a compact, lightweight actuator. Electrohydraulic actuators are attractive as a potential replacement to conventional hydraulic systems in aerospace, automotive, and robotic applications where size and weight are of concern (Alfayad et al., 2011; Anderson et al., 2003; Kim and Wang, 2009). These actuators eliminate the need for hydraulic lines, allowing for power-by-wire systems with reduced weight and improved reliability.

The theoretical power output from a smart material pump is directly proportional to the frequency of operation. Although piezoelectric and magnetostrictive materials are capable of pumping fluid at high-frequencies, designing check valves to perform the fluid rectification above 1 kHz has proven difficult. Early smart material pumps used either commercially available ball-spring valves or custom disc-spring valves, which limited the pumping frequency for peak performance to below 100 Hz (Gerver et al., 1998; Oates and Lynch, 2001). Later designs used valves consisting of a thin metal reed

covering an inlet hole (Chaudhuri and Wereley, 2010; Rupinsky and Dapino, 2006; Sirohi and Chopra, 2003). Using reed valves enabled the performance of smart material electrohydraulic actuators to improve, but the pumping frequency for peak performance has typically been limited to a few hundred hertz.

Single reed-style valves have been the subject of much study for improving the performance of smart material electrohydraulic actuators. Chaudhuri et al. (2009) considered the coupling between fluid flow and valve displacement in a 2-D finite-element analysis of reed valves. Walters (2008) presented flow resistance calculations based on a 3-D computational fluid dynamics model that considered a static reed geometry.

An approach to developing check valves with increased rectification speed is to use an array of miniature valves. Decreasing the size (mass) of each valve while maintaining the stiffness improves the frequency response, while using many valves in an array can

Smart Vehicle Concepts Center, Department of Mechanical and Aerospace Engineering, The Ohio State University, Columbus, OH, USA

Corresponding author:

Marcelo J Dapino, Vehicle Concepts Center, Department of Mechanical and Aerospace Engineering, The Ohio State University, Columbus, OH 43210, USA.

Email: dapino.1@osu.edu

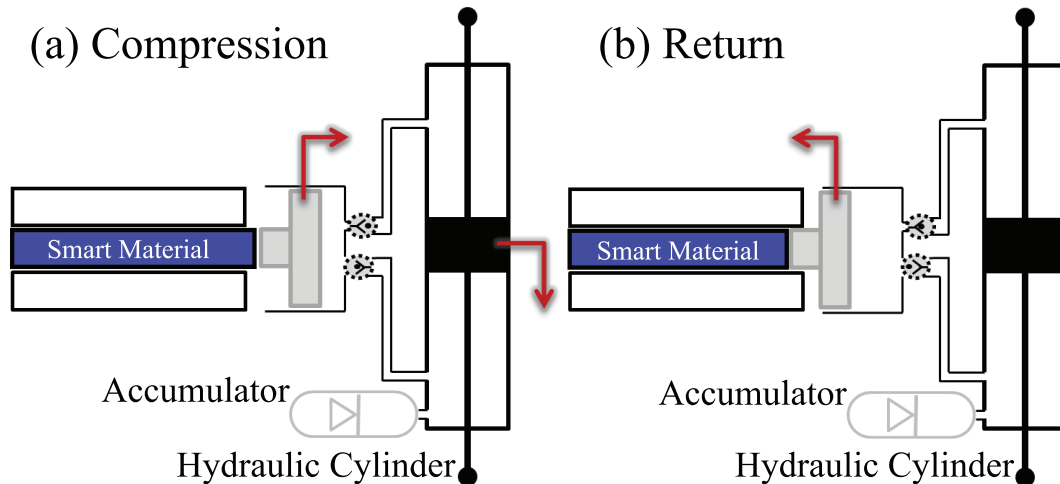


Figure 1. The smart material electrohydraulic actuator principle of operation consists of alternating compression and return strokes of the smart material driver resulting in motion of the hydraulic cylinder.

maintain the flow rate of a larger, single-reed design. Previous attempts to develop miniature valve arrays for hydraulic actuators include silicon valves, nickel valves on a silicon substrate, and all-nickel valves (Lee et al., 2007; Li and Chen, 2005; Li et al., 2005). These valve designs were manufactured using microelectromechanical systems (MEMS) processes to selectively add and remove material to fabricate the different valve layers. The miniature valve array concept was proven to be promising; a pump using the silicon and nickel-silicon valves successfully generated a differential pressure at frequencies above 10 kHz (Li et al., 2005; O'Neill and Burchfield, 2007). However, the silicon valves were found to quickly fail when tested at pump pressures, and the nickel valves produced unacceptably high reverse flows because of fabrication defects (O'Neill and Burchfield, 2007). Seong et al. (2008) used nitinol to design a miniature valve array with large valve openings by taking advantage of the high strains (up to 10%) available due to the pseudoelastic effect. Testing was limited to static flow conditions; fatigue-life considerations may limit the available strains from nitinol for high-frequency pump applications (Eggeler et al., 2004). Prior to this study, no miniature valve array has been demonstrated to reliably rectify flow in the high-pressure, high-frequency environment of smart pumps.

This article presents a design for a robust miniature-reed valve array. Fatigue-life effects are considered in the design to overcome the limitations of previously published designs. The miniature-reed valve array is characterized via both static and dynamic testing. For comparison, a single-reed design is studied; this larger design allows for the in situ tip displacement to be measured to characterize the dynamic response. A computational fluid dynamics model is used to analyze the fluid–structure interaction between a miniature-reed valve and hydraulic fluid; the model results are

validated with flow resistance and tip displacement measurements. The miniature-reed valve array is shown to successfully rectify flow while surviving the high-pressure and high-frequency pumping conditions.

Actuator principle of operation

The principle of operation for a smart material electrohydraulic actuator is shown in Figure 1. An electrical or magnetic input signal, typically sinusoidal, causes a smart material rod to alternatively extend and contract. The extension stroke compresses the hydraulic fluid, increasing the pressure in the pumping chamber until the outlet check valve opens to allow fluid to move into the output hydraulic cylinder. During the return stroke, the driver contracts to return the piston to its initial position. The outlet check valve maintains the pressure on the high-pressure side of the hydraulic cylinder by preventing backflow while the pumping chamber expands. The pressure in the pumping chamber continues to decrease until it drops below the pressure on the low-pressure side of the hydraulic cylinder. Then, the inlet check valve opens to draw fluid into the pumping chamber to refill it for the next compression stroke. The types of smart materials typically used for these pumps are weak in tension, so an accumulator on the low-pressure side of the hydraulic cylinder maintains a bias pressure to keep the smart material driver in compression during operation and to prevent cavitation. The pumping sequence is repeated at high frequency, producing useful work at the hydraulic cylinder from the short fluid pulses created by the smart material.

Valve design

Miniature-reed valve array

The miniature-reed valve array was designed to fit within an existing electrohydraulic actuator valve port

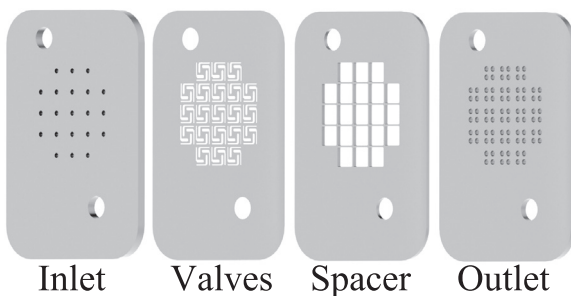


Figure 2. The miniature-reed valve consists of four layers stacked together. Two large holes are provided on each part for alignment pins.

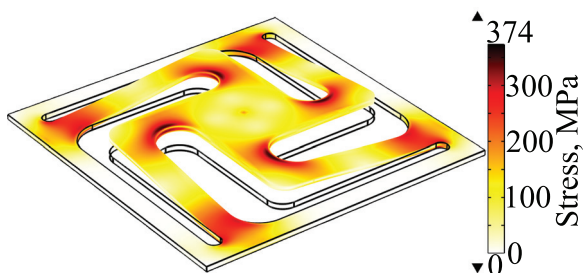


Figure 3. Design stress in fully open miniature reed (25 μm displacement) calculated using a COMSOL finite-element model.

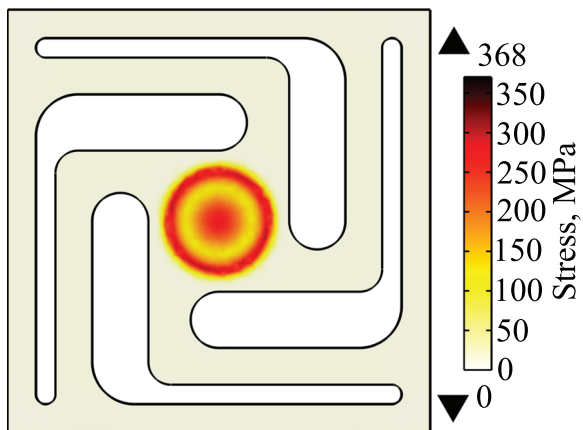


Figure 4. Design stress in the miniature-reed valve while closed, supporting a 10-MPa (1500-psi) pressure.

(Rupinsky and Dapino, 2006) to facilitate comparison with designs based on larger single reeds. The valve port size limited the overall diameter to 6.4 mm (0.25 in), which allowed for only 21 valves in the array. The valve design consists of four layers: inlet, valve, spacer, and outlet (Figure 2). The valve layer contains the valve flaps, which cover holes in the inlet layer. The outlet layer contains both the fluid flow path and stops to limit the travel of the valves. The maximum distance that the valves can open is determined by the thickness of a spacer layer between the valve layer and the outlet

layer. Alignment holes are provided to keep the different layers aligned with pins.

Due to the high-frequency operation of the pump, the valves were designed for a high-cycle fatigue regime. Stainless steel was chosen for the valve material due to its corrosion resistance and well-known fatigue behavior. Unlike materials used in previous miniature-reed designs (such as silicon and nickel), the fatigue strength for austenitic stainless steel is nearly constant above 10^6 cycles (Bathias et al., 2001; Hamrock et al., 1999). This allows for a valve design capable of surviving the high-frequency cycles of pressure generated by the pump.

An allowable stress of 390 MPa (56 ksi) was calculated for the fully hardened stainless steel 301 used in the design (Appendix 1). Two extreme cases were considered for analysis: full valve displacement and blocked pump pressure. The displacement is limited by the thickness of the spacer layer (25 μm), whereas the maximum blocked pressure of the pump was determined in previous experiments to be approximately 10 MPa (1500 psi). A finite-element model was developed using COMSOL Multiphysics to analyze the stress in each of these cases; the design dimensions were optimized to reduce the stress to allowable levels. The maximum stress was calculated to be 374 MPa for full opening and 368 MPa for maximum pump pressure level (Figures 3 and 4).

For successful performance of the pump at frequencies over 1 kHz, the natural frequency of the valve must be higher than this value. The first natural frequency of the valve was calculated as 20.6 kHz in vacuum using COMSOL (Figure 5). During operation, the hydraulic fluid effectively adds mass to the valve, decreasing frequency response. The decreased first natural frequency in the fluid, f_{fluid} , compared to the natural frequency in vacuum, f_{vacuum} , is

$$\frac{f_{\text{fluid}}}{f_{\text{vacuum}}} = \left(1 + \frac{M_{\text{add}}}{M_p}\right)^{-1/2}, \quad (1)$$

where M_p is the mass of the plate and M_{add} is the added mass (Blevins, 1979). The miniature valve geometry can be approximated by a square plate to give $M_{\text{add}} = 0.455\rho l^3$, where ρ is the density of the fluid and l is the length of one of the sides. Equation (1) predicts that the miniature-reed design has a first natural frequency of 14.7 kHz in hydraulic fluid (Mobil DTE 24).

Comparison to single reed

For comparison, a larger single-reed valve design was tested. Rupinsky (2006) described the design process for the single-reed valve in detail; this valve is made from 0.127-mm-thick (0.005 in) stainless steel and is approximately 7 mm long and 5 mm wide. The frequency response of the valve was measured to verify the design calculations for the effect of hydraulic fluid.

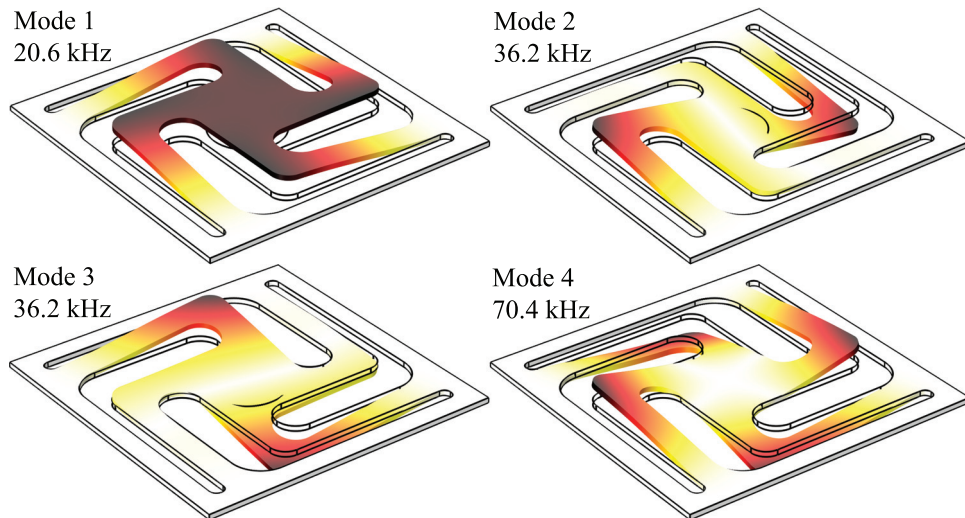


Figure 5. First four mode shapes of the both analytically and experimentally in vacuum. The first mode shape corresponds to the axial motion of the valve necessary for operation. The other modes are at significantly higher frequencies and are not expected to affect valve performance.

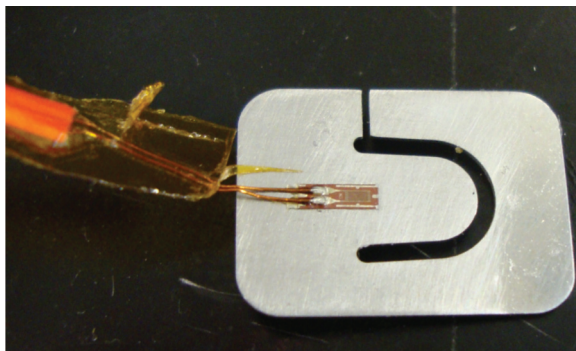


Figure 6. Single-reed valve tested with strain gage affixed for measuring the in situ tip displacement.

Additionally, the single-reed valves were used for comparison testing to the miniature-reed valve array in a smart material actuator.

The expected decrease in natural frequency from the added mass of the surrounding hydraulic fluid was calculated using relation (1). The single-reed valves can be approximated as a cantilever beam with the added mass equal to the fluid mass contained within a swept cylinder of the valve width, that is, $M_{\text{add}} = 0.25\rho\pi l w^2$, where l and w are the length and width of the beam. The frequency response of the single-reed valves was measured by tracking the response to a step displacement. The valves were clamped in a test holder and manually displaced a small amount. This displacement was then released; the valve oscillations returning back to the initial position were measured using both a noncontact laser displacement sensor (Keyence LK-G 32) and a strain gage (Figure 6).

The results of determining the first natural frequency of the single-reed valve in fluid both analytically and experimentally are summarized in Table 1. Adding the strain gage was found to have a negligible effect on the frequency measurement. The 3% difference in the measured natural frequency in air with and without the gage installed can be attributed to a slight variation (less than 0.1 mm) in the clamped length of the valve between tests. The damping ratio was calculated using the log decrement of the response as 0.0036 for the reed in air and 0.076 for the reed in fluid. The results demonstrate that the added-mass factor from equation (1) accounts for the effect of the fluid on the reed valve's dynamic response. The miniature-reed valves, which are too small for testing with conventional strain gages, are expected to exhibit similar behavior.

Fabrication

As designed, the miniature-reed valves consist of 500- μm square flaps with four spring arms. These flaps each cover a 360- μm -diameter hole in the inlet valve layer. The valve and spacer layers were laser cut from a 25-

Table I. Natural frequency of the reed shown in Figure 6, in air and in hydraulic fluid, calculated as damped natural frequency and measured (without and with the strain gage installed).

	f_1 in air (Hz)	f_1 in fluid (Hz)
Calculated	2155	1190
Reed only	2100	N/A
Strain gage installed	2160	1170

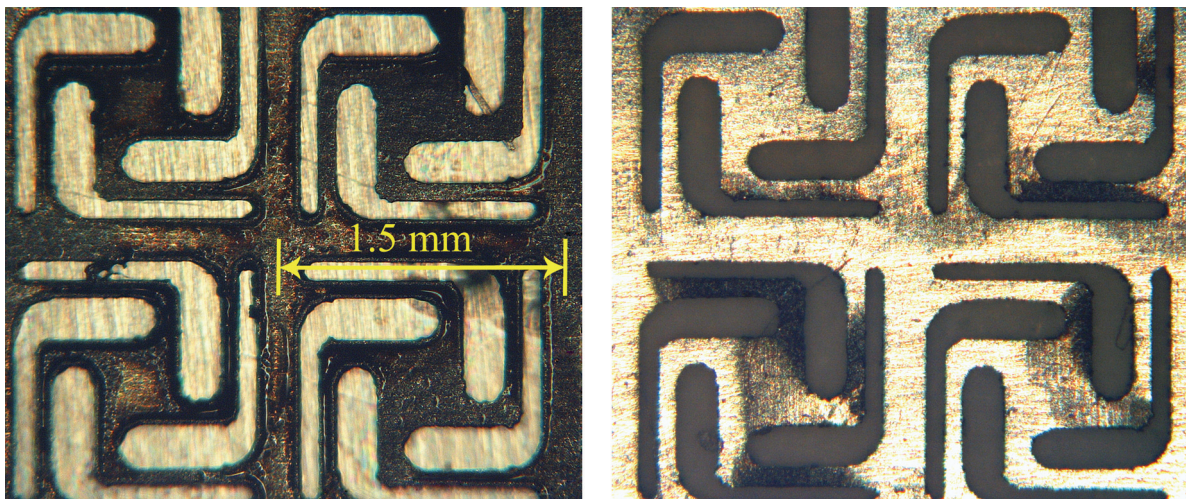


Figure 7. The as-received condition of the miniature reeds had a large amount of oxidation remaining from the laser-cutting process (left). A polishing step removed much of this oxidation (right).

μm -thick stock. The thicker inlet ($700 \mu\text{m}$) and outlet ($300 \mu\text{m}$) layers were fabricated with micromachining processes.

The laser-cutting process was found to leave a large amount of oxidation on the valves. In initial tests on the valves in the as-received condition, the oxidation effectively reduced the spacing distance, which limited the amount that the valves could open and decreased the flow performance. Additionally, the layer of oxidation interfered with the seal between the valve and valve seat, causing significant leakage flow under reverse pressure. Polishing removed much of the oxidation to allow the valves to function as designed (Figure 7).

The stiffness of the miniature-reed valves is calculated to be 8.55 N/mm using COMSOL's 3-D finite-element structural mechanics model (Figure 3). The model geometry was adjusted according to measurements of the reeds to account for fabrication tolerances and material removal from polishing.

Finite-element analysis

To calculate the expected flow performance of the miniature-reed valves, the multiphysics software COMSOL was used. A fluid–structure interaction model was developed based on the geometry of the reed valves. The fluid pressure and the flow distribution along with the resulting valve deformation were solved simultaneously.

Figure 8 shows the geometry for modeling the flow through one of the valves in the array. A 2-D axisymmetric model was used to efficiently predict the flow characteristics of the valve. The 2-D approximation of the valve as a disc is appropriate because most of the pressure drop in the valve takes place underneath the

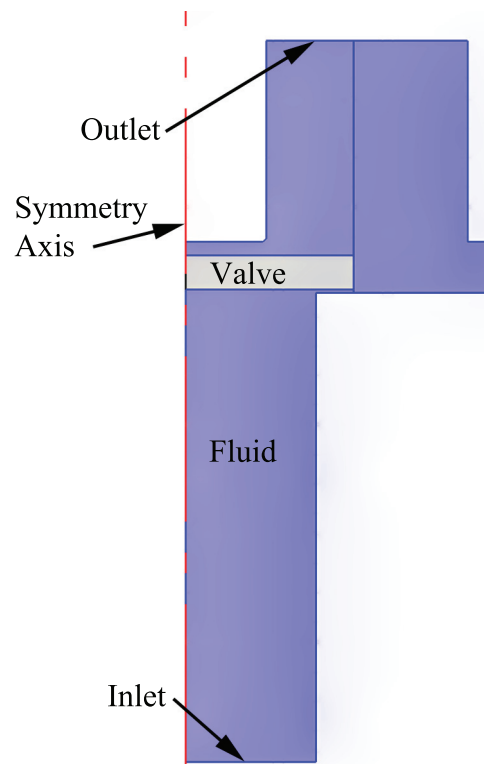


Figure 8. Geometry used for finite-element modeling using COMSOL.

valve seat; the small area of the inlet–valve interface of 0.028 mm^2 at maximum valve opening makes the losses from the inlet (0.1 mm^2) and outlet (0.4 mm^2) areas negligible. The stiffness of the valve was applied to the valve disc as an additional load. A constant pressure differential was applied between the inlet and outlet, and a no-slip condition was applied to the walls. To

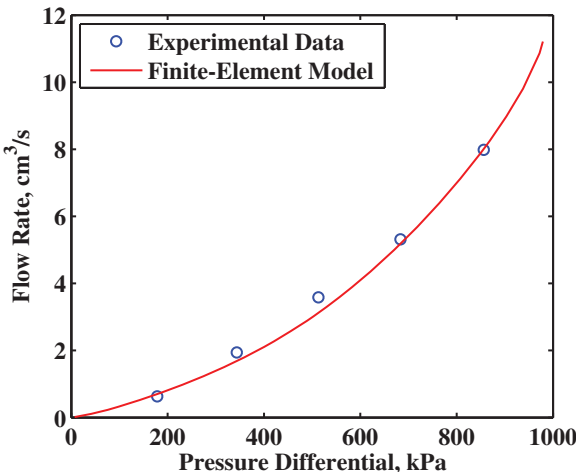


Figure 9. Comparison of steady-state testing results to finite-element model results.

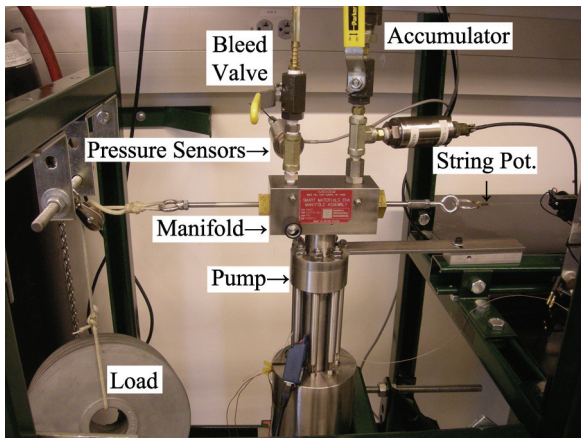


Figure 10. Experimental setup for characterization of the electrohydrostatic actuator.

keep the fluid domain continuous, an offset is needed between the valve and valve seat in the initial geometry. This offset was kept small to minimize its effect on the solution. An Arbitrary Lagrangian–Eulerian (ALE) finite-element formulation was used to deform the mesh and track the motion of the valve with applied pressure. The finite-element modeling results were validated based on static testing of the reed valve.

Experimental study

Steady-state testing

A steady-state flow test was conducted to determine the flow resistance of the valve and validate the finite-element model results. A valve holder was fabricated for the test to match the geometry of the valve port in the pump. A fluid reservoir supplied Mobil DTE 24 hydraulic fluid at a constant pressure, maintained by a

compressed nitrogen cylinder and regulator. The mass flow rate of the fluid was measured with a precision scale, and the pressure differential across the valve was measured using two Sensotec 7351-02 pressure sensors. Testing was conducted up to 900 kPa; the results are compared with the COMSOL finite-element model predictions (Figure 9).

To test for the one-way flow control, a set of tests was conducted with the direction of applied pressure reversed. A small amount of leakage was observed, measuring approximately $0.5 \text{ cm}^3/\text{s}$ over the full range of pressures tested (0–1.4 MPa). The leakage may be attributed to the valves not sealing fully because of the oxidation remaining from the laser-cutting process (Figure 7). Misalignment between the valve flaps and inlet holes may be an additional source of leakage.

Actuator testing

To assess the effect the valves have on overall performance, both the miniature-reed valves and single-reed valves were tested in the smart material actuator (Figure 10). The actuator is driven by a 114-mm-long, 13-mm-diameter Terfenol-D rod with an 860 turn coil. A constant sinusoidal current ($3.5 \text{ A}_{\text{rms}}$) was applied over a range of frequencies; the resulting displacement of the 13-mm bore, 6.4-mm rod hydraulic cylinder was measured. A bias pressure of 2.6 MPa (375 psi) was used for all tests, resulting in a preload of 10.3 MPa (1.5 ksi) on the driver due to the area ratio between the Terfenol-D rod and 25-mm-diameter pumping piston.

Figure 11 compares the unloaded velocity of the smart material actuator with the two different valve designs. The single-reed valve achieved a higher peak velocity of 74 mm/s at 300 Hz, while the miniature array achieved a peak velocity of 33 mm/s at 200 Hz. The performance trends using the two types of valves were similar, but the miniature-reed arrays restrict the flow more than the single-reed valves, resulting in lower velocity.

The blocked pressure, which is the amount of pressure that the pump generates with the hydraulic cylinder fixed, depends less on the flow area than the actuator velocity tests, since the pump can build up pressure over many cycles (Oates and Lynch, 2001; Rupinsky and Dapino, 2006). The blocked pressure was measured up to 2 kHz for a constant $1.4 \text{ A}_{\text{rms}}$ applied sinusoidal current (Figure 12). The resulting blocked pressure for the miniature reeds is approximately two-thirds of the single-reed result for a large portion of the test. This decrease can be attributed to the backflow noted in the miniature reeds during the static tests. The difference is higher at low frequencies, where there is more time for the pressure to bleed off between pump cycles. It is emphasized that the blocked pressure for both types of valves decreases

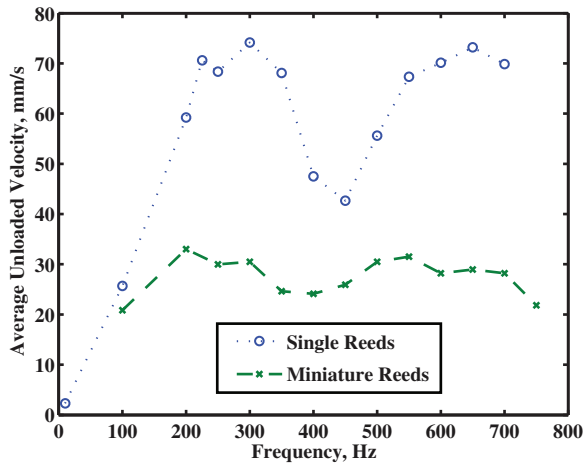


Figure 11. Unloaded test results for pump performance comparing the miniature-reed array to the single-reed valves.

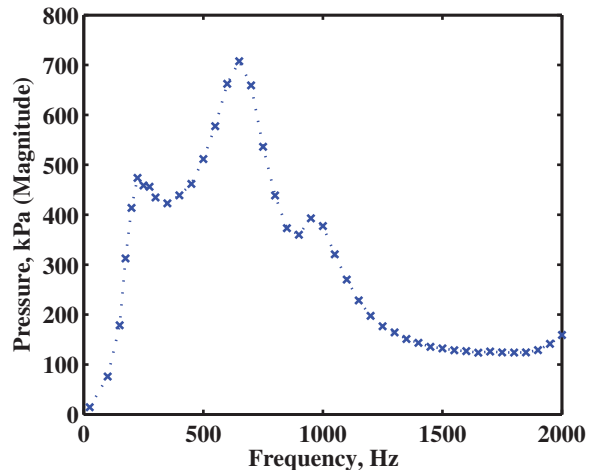


Figure 13. Magnitude of the blocked pressure response for the system without valves installed for a constant sinusoidal current ($1.4 \text{ A}_{\text{rms}}$).

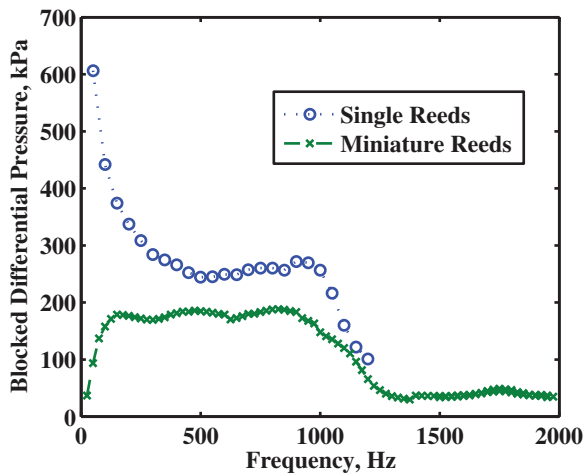


Figure 12. Blocked pressure results from a low-current ($1.4 \text{ A}_{\text{rms}}$) sinusoidal frequency sweep of the pump input comparing both types of valves.

rapidly at frequencies above 1000 Hz, indicating that a common factor is attenuating the pressure at high frequencies.

To isolate the effect of the pump manifold on the test results, the blocked test procedure was repeated without any valves installed. The amplitude of the pressure variation was measured since a differential pressure is not generated without the valves (Figure 13). The results below 1000 Hz show a double-peaked response, with peaks in the measured pressure response corresponding to the peaks in the unloaded actuator velocity tests (225 Hz and 650 Hz). Above 1000 Hz, there is a sharp decrease in the measurement, which matches the reduction in response in the tests with the valves installed. This indicates that the manifold and pump, rather than the valves, limit the bandwidth of this actuator design.

Conclusion

A new design for miniature-reed valves, with each layer machined separately using micromachining processes, successfully rectifies fluid flow in a smart material electrohydraulic actuator. This has not been shown in other miniature-reed designs that have been proposed, which failed when tested in a smart material pump or were designed and tested using only static considerations. The design was proven to be robust, effectively surviving operation at high-pressure and high-frequency inside the pump. The pump data shown represents a large number of actuation cycles (Figure 11 alone represents over 30,000 cycles), consistent with the fact that the valves were designed using a stainless steel that allows for an infinite-life approach. The measured flow rates from the miniature-reed valves are lower than the flow rates for the single-reed valves, but this is expected because the miniature-reed array design utilizes the existing valve ports at a penalty of greatly reduced available flow area. The flow restriction of the valves could be reduced simply by using a larger number of valves in the array (Lee et al., 2007; Li and Chen, 2005; Seong et al., 2008). The area of the pump piston is approximately eight times the area of the inlet and outlet reeds combined (507 mm^2 vs. 63 mm^2), so a pump designed specifically for a miniature-reed array could utilize significantly more valves without increasing the overall size of the system.

A fluid–structure interaction finite-element model for valve flow resistance has been established, and the results verified using steady-state measurements of flow through the valve array. Dynamic testing of the single-reed valve design confirmed the analytical design calculations for the added-mass effect of the hydraulic fluid on the frequency response of reed valves. These design tools can be used to optimize future valve designs. It

was determined that the pump and manifold used for testing limited the frequency response of the system. Optimizing the manifold passage geometry to support high-frequency fluid flow will be necessary to fully utilize the miniature-reed valve design and improve the performance of the smart actuator.

Funding

Financial support for this research was provided by the Smart Vehicle Concepts Center, a National Science Foundation Industry/University Cooperative Research Center (www.SmartVehicleCenter.org), and by the Ohio State University through a Smart Vehicle Concepts Graduate Fellowship. Technical advice was provided by Thomas Greetham and Thomas Walters of Moog, Inc. (East Aurora, NY). This work was supported in part by an allocation of computing time from the Ohio Supercomputer Center.

References

- Alfayad S, Ouezdou FB, Namoun F, et al. (2011) High performance integrated electro-hydraulic actuator for robotics-part I: principle, prototype design and first experiments. *Sensors and Actuators A: Physical* 169(1): 115–123.
- Anderson E, Bales G and White E (2003) Application of smart material-hydraulic actuators. *Proceedings of SPIE* 5054: 73.
- Bathias C, Drouillac L and Le Francois P (2001) How and why the fatigue S–N curve does not approach a horizontal asymptote. *International Journal of Fatigue* 23: 143–151.
- Blevins RD (1979) *Formulas for Natural Frequency and Mode Shape*. Van Nostrand Reinhold Company, New York.
- Chaudhuri A and Wereley NM (2010) Experimental validation of a hybrid electrostrictive hydraulic actuator analysis. *Journal of Vibration and Acoustics* 132(2): 021006.
- Chaudhuri A, Yoo JH and Wereley NM (2009) Design, test and model of a hybrid magnetostrictive hydraulic actuator. *Smart Materials and Structures* 18: 085019.
- Eggeler G, Hornbogen E, Yawny A, et al. (2004) Structural and functional fatigue of NiTi shape memory alloys. *Materials Science and Engineering A* 378(1–2): 24–33.
- Gerver M, Goldie J, Swenbeck J, et al. (1998) Magnetostrictive water pump. *Proceedings of SPIE* 3329: 694–705.
- Hamrock B, Jacobson B and Schmid S (1999) *Fundamentals of Machine Elements*. New York: WCB/McGraw-Hill.
- Keller CA (2004) *Novel concepts in piezohydraulic pump design*. Master's Thesis, Georgia Institute of Technology, Atlanta, GA.
- Kim G and Wang K (2009) Switching sliding mode force tracking control of piezoelectric-hydraulic pump-based friction element actuation systems for automotive transmissions. *Smart Materials and Structures* 18(8): 085004.
- Lee D, Shin D and Carman G (2007) Large flow rate/high frequency microvalve array for high performance actuators. *Sensors and Actuators A: Physical* 134(1): 257–263.
- Li B and Chen Q (2005) Design and fabrication of in situ UV-LIGA assembled robust nickel micro check valves for compact hydraulic actuators. *Journal of Micromechanics and Microengineering* 15(10): 1864.
- Li B, Chen Q, Lee D, et al. (2005) Development of large flow rate, robust, passive micro check valves for compact piezoelectrically actuated pumps. *Sensors and Actuators A: Physical* 117(2): 325–330.
- Oates WS and Lynch CS (2001) Piezoelectric hydraulic pump system dynamic model. *Journal of Intelligent Material Systems and Structures* 12(11): 737–744.
- O'Neill C and Burchfield J (2007) Kinetic ceramics piezoelectric hydraulic pumps. *Proceedings of SPIE* 6527: 65270I.
- Rupinsky MJ (2006) *Smart material electrohydrostatic actuator for intelligent transportation systems*. Master's Thesis, The Ohio State University, Columbus, OH.
- Rupinsky MJ and Dapino MJ (2006) Smart material electrohydrostatic actuator for intelligent transportation systems. *ASME Conference Proceedings* 47683: 721–730.
- Seong M, Mohanchandra K, Lin Y, et al. (2008) Development of a 'bi-layer lift-off' method for high flow rate and high frequency Nitinol MEMS valve fabrication. *Journal of Micromechanics and Microengineering* 18: 075034.
- Sirohi J and Chopra I (2003) Design and development of a high pumping frequency piezoelectric-hydraulic hybrid actuator. *Journal of Intelligent Material Systems and Structures* 14(3): 135–147.
- Walters T (2008) *Development of a smart material electrohydrostatic actuator considering rectification valve dynamics and in situ valve characterization*. Master's Thesis, The Ohio State University, Columbus, OH.

Appendix I

Allowable stress calculation

The endurance limit for the stainless steel used in the miniature-reed valve design was calculated using the method outlined by Hamrock et al. (1999). It was noted that the maximum stress in the reed occurs in torsion of the arms that extend from the reed flap, so the uncorrected endurance limit, S'_e , was calculated for torsion loading based on the ultimate strength of the material, S_u

$$S'_e = 0.29S_u. \quad (2)$$

The endurance limit, S_e , is then modified using correction factors for surface finish, k_f ; size, k_s ; reliability, k_r ; and temperature, k_t

$$S_e = k_f k_s k_r k_t S'_e. \quad (3)$$

The allowable stress is then equal to twice the alternating stress, calculated from the modified Goodman criterion using a mean stress equal to the alternating stress (Keller, 2004)

$$\sigma_{\text{allow}} = 2\sigma_a = 2S_e \left(1 + \frac{S_e}{S_u}\right)^{-1}. \quad (4)$$

To calculate the allowable stress for the valve design, an ultimate strength of 1280 MPa was assumed for fully hardened 301 stainless steel. The surface finish factor was set to $k_f = 0.75$ based on the expected surface

roughness from discussion with the supplier. The reliability factor was set to $k_r = 0.82$ based on 99% reliability. The size and temperature factors were set to 1 because the valves are small, and testing was conducted at room temperature. This resulted in an allowable stress of 390 MPa for the design of the miniature

valves. The allowable stress value is conservative since the material actually used for fabrication was certified to have a higher ultimate strength than used for design, $S_u = 1386$ MPa (fully hardened 304 stainless steel from Trinity Brand Industries).